A&A 369, 646–659 (2001)
DOI: 10.1051/0004-6361:20010120

Astronomy & Astrophysics

Empirical models of solar magnetic flux-tubes and their non-magnetic surroundings

C. Frutiger[1] and S. K. Solanki[2]

[1] Institute of Astronomy, ETH-Zentrum, 8092 Zürich, Switzerland
[2] Max-Planck-Institut für Aeronomie, 37191 Katlenburg-Lindau, Germany

Received 21 July 2000 / Accepted 12 January 2001

Abstract. A powerful method for the analysis of the structure of small scale magnetic elements in the solar photosphere is the inversion of Stokes spectra. In previous papers based on such inversions Bellot Rubio et al. (1997, 1999) and Frutiger et al. (1999) have argued in favor of models with rather different dynamic properties. In this paper we return to this debate and compare results returned by inversions based on new multi-component models applied to several Fe I, Fe II and C I spectral line profiles obtained in active region plage with a Fourier Transform Spectrometer. These inversions differ from earlier ones by the fact that mass conservation is strictly imposed both inside the magnetic elements and on the surrounding external flow field. These flux-tube models are not only able to reproduce the characteristic Stokes V asymmetries and line-shifts observed in active regions plages or network elements, but also the Stokes I line profiles, including line bisectors. It is confirmed that from the quality of the fits alone it is not possible to distinguish between the steady flow proposed by Bellot Rubio et al. (1997) and the oscillatory model of Frutiger & Solanki (1998). If, however, physical constraints are imposed (e.g. mass conservation or that the flow retains the same direction over height in the flux tube) then the oscillatory model is found to be superior. In addition, the current investigation also provides the first inversion-based model of abnormal granulation.

Key words. polarization – radiative transfer – Sun: faculae, plages – Sun: granulation – Sun: magnetic fields

1. Introduction

One of many remarkable features of the solar photosphere is the presence of magnetic fields concentrated in tube-like structures of very different sizes. Sunspots, the largest such structures with a diameter of several thousand kilometers, are well resolved by today's telescopes, but it is unclear whether even the largest telescopes can as yet resolve the finest magnetic flux concentrations. The physical structure of these small-scale magnetic elements in the photosphere plays an important role for the understanding of a number of aspects of solar magnetic activity, e.g., the interacting of the sun's magnetic field with convection, the heating of the solar chromosphere and the process leading to global irradiance variations. In this paper we concentrate on the magnetic elements and their surrounding granules in active region plages. They have been the topic of numerous studies during the past decade. For example, Title et al. (1992) investigated the differences between plages and the quiet sun, Bernasconi et al. (1995) considered the flux tube inclination, Márquez et al. (1996) modeled spectral line asymmetries, Pillet et al. (1997) deduced the properties of the plage magnetic field, while the dynamic behavior of the plasma within magnetic elements was studied by Steiner et al. (1998) and Grossmann-Doerth et al. (1998) on the basis of MHD simulations and by Sigwarth et al. (1999) from Stokes Spectra. The lack of direct observational information on the internal structure of the small-scale magnetic elements is bridged by introducing models of the unresolved features. Inversion methods based on such simplified model atmospheres have repeatedly been shown to be an effective means of deriving the photospheric structure in facular regions or plages, e.g. Sánchez Almeida (1997), Bellot Rubio et al. (1997, 1999) (hereafter BRC97, BRC99), Frutiger & Solanki (1998); Frutiger et al. (1999) (hereafter FS98, FSFB99), or network and intra-network regions (Almeida & Lites 2000).

A problem of particular interest that has been less than satisfactorily understood is the origin of the asymmetric shapes of the observed Stokes V profiles and zero-crossing wavelength shifts. Different approaches have been proposed (cf. Illing et al. 1975; Grossmann-Doerth et al. 1989; Solanki 1989; Sánchez Almeida et al. 1989 and references therein). The inversion approach presented by BRC97 assuming a 2-component flux-tube model is able to reproduce the Stokes profiles of two Fe I lines observed with the Advanced Stokes Polarimeter (Pillet et al. 1997) with great accuracy. In addition, BRC99 showed

Send offprint requests to: C. Frutiger,
e-mail: frutiger@astro.phys.ethz.ch

that this model is able to reproduce the zero-crossing Stokes V line-shifts of about 100 Fe I and 16 Fe II line profiles recorded in active region plages with the Fourier Transform Spectrometer on Kitt Peak by Stenflo et al. (1984). However, this model apparently suffers from mass-conservation problems within the magnetic flux tube since it returns fast downflows in the interior of the magnetic element as well as in the non-magnetic surroundings. The downflows resulting from these inversions imply gas flux across field lines orders of magnitude in excess of that expected on the basis of the conditions found in the solar photosphere (Hasan & Schüssler 1985).

In order to overcome these problems one could assume that either the BRC97 model is geometrically incomplete (e.g. that the magnetic flux in the flux tube returns to the solar surface in the form of a relatively weak field harboring an upflow) or that it describes only a single phase of a dynamic development. Following this line of reasoning FS98 and FSFB99 proposed an oscillatory model for the interior of the magnetic elements that guarantees mass conservation within the flux tubes and also reproduces the observational data. However, even in this case mass conservation is not properly imposed on the external gas. A completely different approach is proposed by Sánchez Almeida (1997) and Almeida & Lites (2000), who consider mass conservation inside the magnetic features with height but not in time. Again, the observational data are well reproduced. This model relies on the assumption that the magnetic field is concentrated in elements with diameters of only a few kilometers. Even the next generation of telescopes will probably not be able to spatially resolve such small structures (the classical flux-tube models assume a tube diameter of the order of 100 km at $\tau_{5000} = 1$).

In the present paper we reinvestigate the structure of flux tubes in active region plages using a new 4-component model. This model introduces not only the physically sensible constraint of mass-conservation within the magnetic elements but also takes into account the presence of convective up- and downflows in the field-free surroundings (see Bünte et al. 1993; Briand & Solanki 1998). While the magnetic interior determines the basic properties of the polarized light emerging from the observed region (essentially Stokes V at disk center), it is only the combination of the motion of the plasma within the magnetic elements and in the immediate field-free surroundings that is able to produce Stokes V profiles showing the typically observed amplitude- and area asymmetries (Grossmann-Doerth et al. 1989; Solanki 1989). On the other hand, the contributions to the total intensity profiles are dominated by the non-magnetic (upflowing) plasma further away from the magnetic elements. With this in mind we impose a simple mass-conservation scheme on the gas outside the magnetic elements. It links the fast downflows along the magnetic flux tubes with the granular upflows further away from the tube axis.

In an attempt to provide stronger constraints than given by the two lines generally employed for inversions based on response functions we fit a large number of lines, including lines of C I that are formed deep in the photosphere and thus constrain the continuum-forming layers.

2. Observational and atomic data

For our analysis we use the high-spectral resolution Fourier Transform Spectrometer (FTS) measurements of Stenflo et al. (1984) of two different plage regions. The spectra are corrected for gravitational redshift, for the Sun-Earth relative motion and for solar rotation (Solanki 1986). The relevant data sets have been referred to as FTS4 and FTS5 in the past (Solanki 1987). The spatial resolution of these data is 10 arcsec and the integration time is 21–35 min, which should be borne in mind when constructing and interpreting the model atmospheres.

Table 1 lists the spectral lines employed for the inversions of the two data sets, as well as the adopted atomic parameters. We employ both Fe I and Fe II lines due to their different temperature sensitivities and formation heights (cf. Solanki & Stenflo 1985). The weak, high-excitation C I lines have been used with the goal of improving the determination of the temperature in the continuum forming layers of the magnetic elements (cf. Solanki & Brigljević 1992). Column (2) gives the laboratory wavelengths. For Fe I lines they are taken from Nave et al. (1994). The laboratory wavelengths of Fe II lines available to us are generally less accurate, so that the wavelengths of these lines are treated as free parameters following Bellot Rubio et al. (1999). Column (3) gives the energy of the lower level of the transition adopted from Sugar & Corliss (1985). Column (4) gives the enhancement factors E over the values of the damping constant calculated using the simple Unsöld formula and Van der Waals broadening theory (at $T = 5000$ K). For Fe I the collisional damping parameters are derived from the cross-sections recently presented by Anstee & O'Mara (1995), Barklem & O'Mara (1997) and Barklem et al. (1998). The values for Fe II lines are estimates. Column (5) lists the oscillator strengths, $\log gf$. Their sources are given below the table. Columns (6) and (7) give the Landé factor of the lower and upper level of the transition adopted from the Kurucz line list. Finally, Cols. (8) and (9) list the effective Landé factors (cf. Mathys 1990) used for the inversion and values assuming LS-coupling, respectively.

3. Inversion code, model atmosphere

Our inversion code is based on a non-linear Levenberg-Marquardt least-squares fitting algorithm, a Hermitian method for the solution of the radiative transfer equation (cf. Bellot Rubio et al. 1998) and response functions for an efficient computation of derivatives of spectral line profiles with respect to the free parameters (cf. Landi Degl'Innocenti 1976; Ruiz Cobo & Del Toro Iniesta 1992). A similar code has earlier been presented by the group around B. Ruiz Cobo (e.g. Bellot Rubio et al. 1997, and references therein). Some important details of our code have been described by Frutiger et al. (2000).

Table 1. Atomic data of the inverted spectral lines

(1) Ion	(2) $\lambda^1_{\rm lab}$ [Å]	(3) $\chi_{\rm e}$ [eV]	(4) E^2	(5) $\log gf$	(6) $g_{\rm l}$	(7) $g_{\rm u}$	(8) $g_{\rm eff}$	(9) $g_{\rm eff,LS}$
FTS4: (4524 Å-5580 Å)								
Fe I	4690.1380	3.6866	1.963	-1.68^3	2.487	1.826	2.157	2.750
Fe I	4704.9481	3.6866	1.961	-1.57^3	0.000	2.487	2.500	2.500
Fe I	4726.1370	2.9982	2.242	-3.25^3	1.908	1.503	2.313	2.333
Fe I	5217.3893	3.2114	2.230	-1.07^4	1.508	1.502	1.517	1.500
Fe I	5243.7769	4.2565	2.253	-1.150^3	1.244	1.287	1.351	1.500
Fe I	5247.0504	0.0873	3.354	-4.946^3	1.500	1.746	1.992	2.000
Fe I	5250.2098	0.1213	3.256	-4.938^3	0.000	2.999	2.999	3.000
Fe I	5250.6460	2.1979	1.829	-2.05^3	1.820	1.661	1.502	1.500
Fe I	5295.3121	4.4156	2.316	-1.69^3	0.887	0.484	0.685	0.708
Fe II	*5132.666*	2.8067	*2.0*	-4.18^3	1.307	1.430	1.369	1.384
Fe II	*5197.570*	3.2307	*2.0*	-2.10^3	0.574	0.445	0.671	0.700
Fe II	*5234.625*	3.2215	*2.0*	-2.22^5	0.980	1.069	0.869	0.929
Fe II	*5264.812*	3.2307	*2.0*	-3.23^5	0.574	1.150	0.142	0.100
C I	4775.8980	7.4878	*1.0*	-2.163^6	–	–	–	1.500
C I	5052.1670	7.6848	*1.0*	-1.303^6	–	–	–	1.000
C I	5380.3370	7.6848	*1.0*	-1.616^6	–	–	–	1.000
FTS 5: (5254 Å-6907 Å)								
Fe I	5506.7791	0.9902	2.332	-2.797^3	1.000	1.500	2.000	2.000
Fe I	5569.6181	3.4172	2.286	-0.486^4	1.004	1.518	0.747	0.750
Fe I	6151.6181	2.1761	2.057	-3.299^3	1.666	1.495	1.837	1.833
Fe I	6252.5554	2.4042	2.030	-1.687^3	1.163	1.248	0.951	1.083
Fe I	6301.5012	3.6537	2.298	-0.718^4	1.835	1.503	1.669	1.667
Fe I	6302.4936	3.6866	2.313	-1.203	2.487	0.0	2.487	2.500
Fe I	6481.8703	2.2788	2.126	-2.984^3	1.506	1.495	1.501	1.500
Fe II	*6149.258*	3.8895	*2.0*	-2.724^5	0.003	2.700	1.352	1.333
Fe II	*6432.580*	2.8912	*2.0*	-3.51^5	1.996	1.653	1.825	1.829
Fe II	*6516.080*	2.8912	*2.0*	-3.38^5	1.996	1.584	1.069	1.071

References: [1]Moore (1970), Nave et al. (1994), Kurucz & Bell (1995); [2]Anstee & O'Mara (1995), Barklem & O'Mara (1997), Barklem et al. (1998); [3]Fuhr et al. (1988), Kurucz & Bell (1995); [4]Bard et al. (1991), Bard & Kock (1994); [5]Schnabel et al. (1999); [6]Miller et al. (1974), Kurucz & Bell (1995).

In this paper we concentrate on the main aspects in which our inversions differ from earlier ones: the multi-component modeling of magnetic elements, in particular the velocities inside and outside the magnetic flux tubes. In order to put additional constraints on the determination of the many free parameters in our models, we employ a larger number of spectral lines (16 in the case of FTS4) than previously employed for this kind of inversion.

Figure 1 shows a vertical cut through the photosphere of part of a schematic active region which illustrates the main features of our 4-component model. The basic idea is to divide the atmosphere into magnetic components expanding with height (flux tubes) and field-free components harboring either a downflow (along the tube boundaries), a predominately horizontal flow or an upflow (further away from the flux tubes). For each of these components, except for the component harboring a horizontal flow, the stratification of the fundamental physical quantities (e.g. temperature, line-of-sight velocity) is modeled by a set of depth-dependent free parameters. The magnetic field strength at the reference height $z = 0$ (corresponding to the average quiet Sun $\tau_{5000} = 1$, where τ_{5000} is the continuum optical depth at 5000 Å) is also a free parameter, as are the individual fractional areas

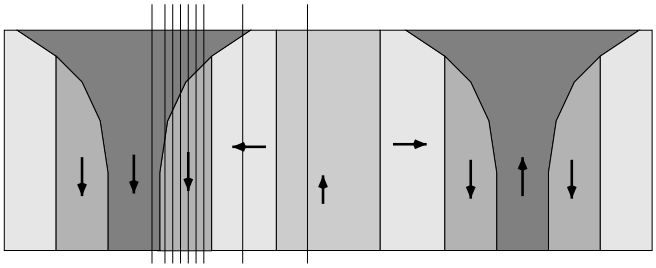

Fig. 1. Vertical cut through schematic small-scale magnetic elements (dark area, expanding with height) and their surroundings as modeled by a 4-component model. The arrows indicate the direction of the mass flow in each component. Long thin lines depict a sample of lines of sight or rays along which the radiative transfer equations are solved

harboring a magnetic field and/or different kinds of velocity (at the same height). Quantities like the micro- or macro-turbulence are also free but assumed to be depth independent. The stratification of the remaining quantities is obtained by assuming LTE, a solar mix of elements and hydrostatic equilibrium (to derive the gas pressure, electron pressure and continuum opacity, Gustafsson 1973), or by using the thin-tube approximation (to derive the magnetic field, Defouw 1976). The physical quantities of the component harboring a horizontal flow are obtained by averaging the quantities from the neighboring field-free up- and downflow components. Consequently we refer to this new model as a 4-component model.

The synthetic spectra $\boldsymbol{S} = (I, Q, U, V)^T$, where I, Q, U and V are the four Stokes parameters (cf. Rees et al. 1989), are obtained by solving the Unno-Rachkovsky equations along a set of 22 vertical rays that sample all components. Most of the rays cut the flux tube at different heights (see Fig. 1). Since the observations do not resolve the individual components we need to average the synthetic spectra over all the rays. The final synthetic Stokes vector $\boldsymbol{S}$ of the 3-component models can thus be written as:

$$\begin{aligned}\boldsymbol{S} \;=\; & (1-\alpha_{\rm up}) \sum_{i=1}^{N_{\rm R}-2} w_i\, \boldsymbol{S}_i \\ & +\alpha_{\rm up}\left(\alpha_{\rm hor}\; \boldsymbol{S}_{\rm hor} + (1-\alpha_{\rm hor})\, \boldsymbol{S}_{\rm up}\right).\end{aligned} \tag{1}$$

The sum over the first $N_{\rm R} - 2$ rays corresponds to the classical thin-tube model composed of a magnetic component and a field-free downflow component (each spectrum $\boldsymbol{S}_i$ calculated along a particular ray is weighted with w_i according to the area it samples), while the other two rays take into account the contribution from the remaining part of the field-free surroundings (i.e. the surface fraction harboring the upflow and the horizontal flow is $\alpha_{\rm up}$). We are aware of the shortcomings of this scheme, which was chosen for its simplicity, and that further improvements are necessary. Nevertheless, extensive tests have shown that restricting ourselves to a single ray each for the horizontal and upflowing external velocity field has little effects on the final result, mainly because the heights at which the flux-tube boundary intersects these parts of the atmosphere almost always lie above the formation heights of most lines in our sample.

In the components of the model described so far, the flux tube cannot satisfy mass conservation in its interior, except in the trivial case of no internal flow. This version of the model is similar to that of BRC97 extended to include the upflow component of the granular velocity field. In the following we refer to it as the 3-component model (since the horizontal component is determined by the properties of the up- and downflowing components).

A second flux-tube component with oppositely directed velocity is required in order to ensure mass conservation (see Fig. 1). The extension to the calculation of synthetic Stokes profiles for two flux tubes is straightforward. The final synthetic profiles $\boldsymbol{S}$ of the 4-component model are given by

$$\boldsymbol{S} = (1-\alpha_{\rm mix})\, \boldsymbol{S}_1 + \alpha_{\rm mix}\, \boldsymbol{S}_2. \tag{2}$$

Here $\boldsymbol{S}_1$ and $\boldsymbol{S}_2$ are each calculated according to Eq. (1), under the condition that both flux-tubes are embedded in the same field-free surroundings, and $\alpha_{\rm mix}$ is a new free parameter determining the relative area coverage of the two types of flux tubes.

The basic properties of the new 4-component model are as follows:

Flux-tube interior:
: No mass is allowed to flow across flux-tube boundaries. Mass conservation with height is imposed (the product of the flow speed, the gas density and the flux-tube cross section does not vary with height) and it is required that the mass flowing upward within a given flux tube must flow down in another flux tube (or in the same flux tube at a later time). The two types of flux tubes harboring oppositely directed flows have the same magnetic flux. This constraint is chosen on the basis of its simplicity. It fits well into the scenario where the two types of flux tubes represent two phases of an oscillation. For spatially coexisting flux tubes the quality of the fits can be used as a validation for this assumption.

Field-free surroundings:
: The granular flow is divided into a downflow along the tube boundaries, a horizontal flow and an upflow region. Averaged horizontally no net vertical mass flow is allowed at any height, i.e. the flow speed times the gas density times the filling factor (which for the atmosphere embracing the flux tubes varies with height) may be height-dependent but is equal in the up- and downflow area. Again, this treatment reduces the number of free parameters. For the upflow region only the temperature stratification and the micro-turbulence are free parameters, all other physical quantities are derived from the downflow properties.

Note that for the inversions presented here we set $\alpha_{\rm hor} = 0$, i.e. the horizontal component in not employed. Tests have shown that this restriction has no significant effect on the results, much as a horizontal component had little effect on the inversion of quiet Sun data carried out by Frutiger et al. (2000). We have retained the option of a horizontal flow in the code, however, since it could turn out to be important for future inversions (e.g. near the limb, cf. Bünte et al. 1993).

The different models used for the inversions presented in the next section are summarized in Table 2. Column (1) gives the designation, Col. (2) the number of components. In Col. (3) the characteristic properties of the velocity stratification inside the flux tubes are summarized. Here $v_{\rm ft}(z)$ signifies the height-dependent line-of-sight velocity within the flux tube. In the 4-component model the subscripts 1 and 2 distinguish between the two flux-tubes,

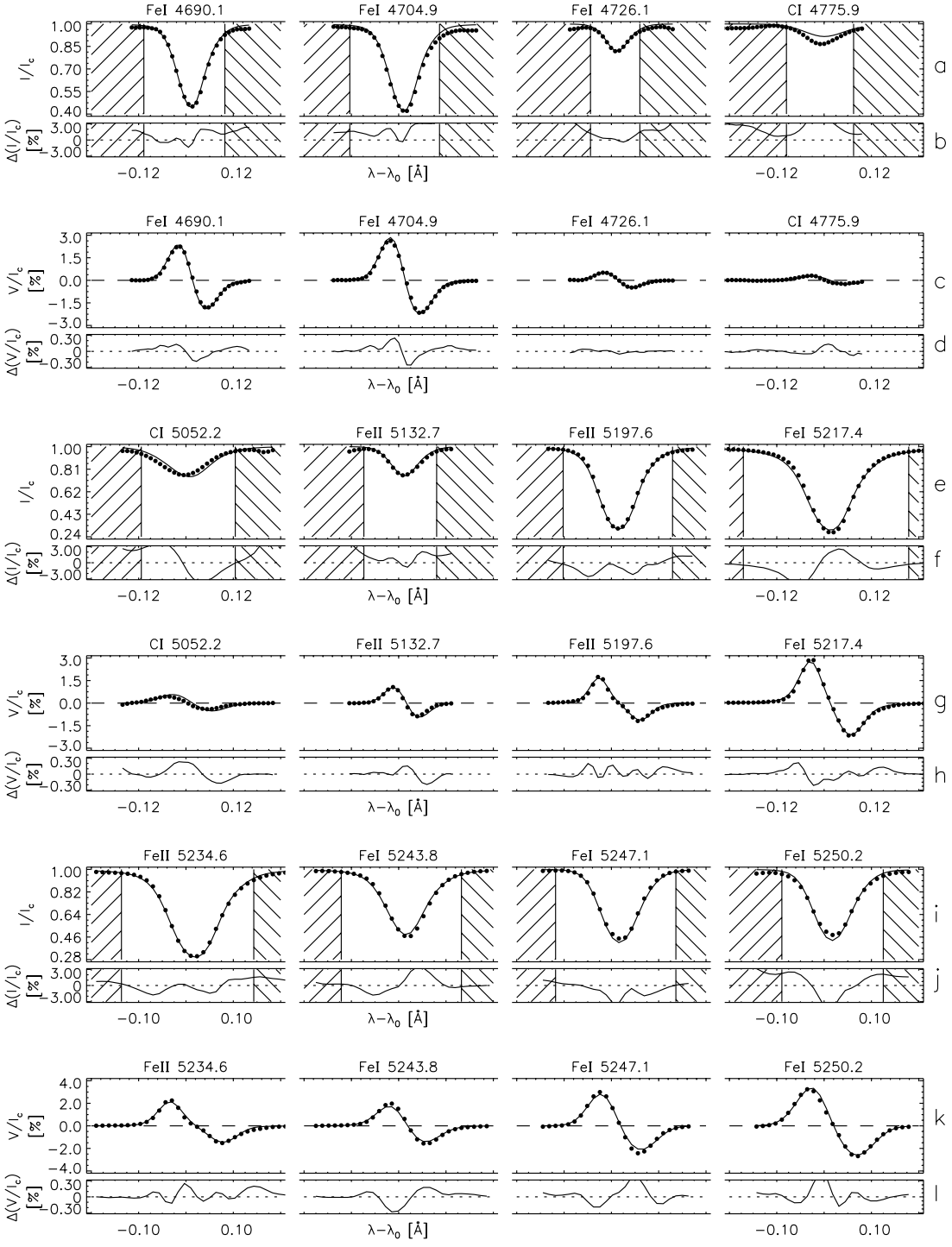

Fig. 2. Observed and best-fit Stokes I/I_c and V/I_c profiles obtained from model A (here I_c is the continuum intensity). In rows **a, c, e, g, i)** and **k)** thin curves refer to the synthetic spectra, dots to the observed spectra taken from the FTS4 data set. Only the portions of the I spectrum between the shaded areas are fit. The rows **b, d, f, h, j)** and **l)** show the differences between the synthetic and observed profiles on a scale stretched by a factor of 100 for clarity (only 12 of the 16 fitted lines are plotted)

while $f(z)$ is a function which ensures that mass conservation is satisfied. It depends on the density, $\rho(z)$, the cross-section, $r^2(z)$, and the weight (surface fraction) of the two flux tubes:

$$f(z) = -\frac{\rho_1(z)}{\rho_2(z)} \frac{r_1(z)^2}{r_2(z)^2} \frac{1-\alpha_{\rm mix}}{\alpha_{\rm mix}}. \quad (3)$$

The minus sign ensures that the gas flows in opposite directions within the two flux tubes.

The 3-component models are very similar to the 4-component model with the basic exception that there is only one type of magnetic flux tube. Model B is similar to models presented earlier by BRC97, BRC99, FS98 and

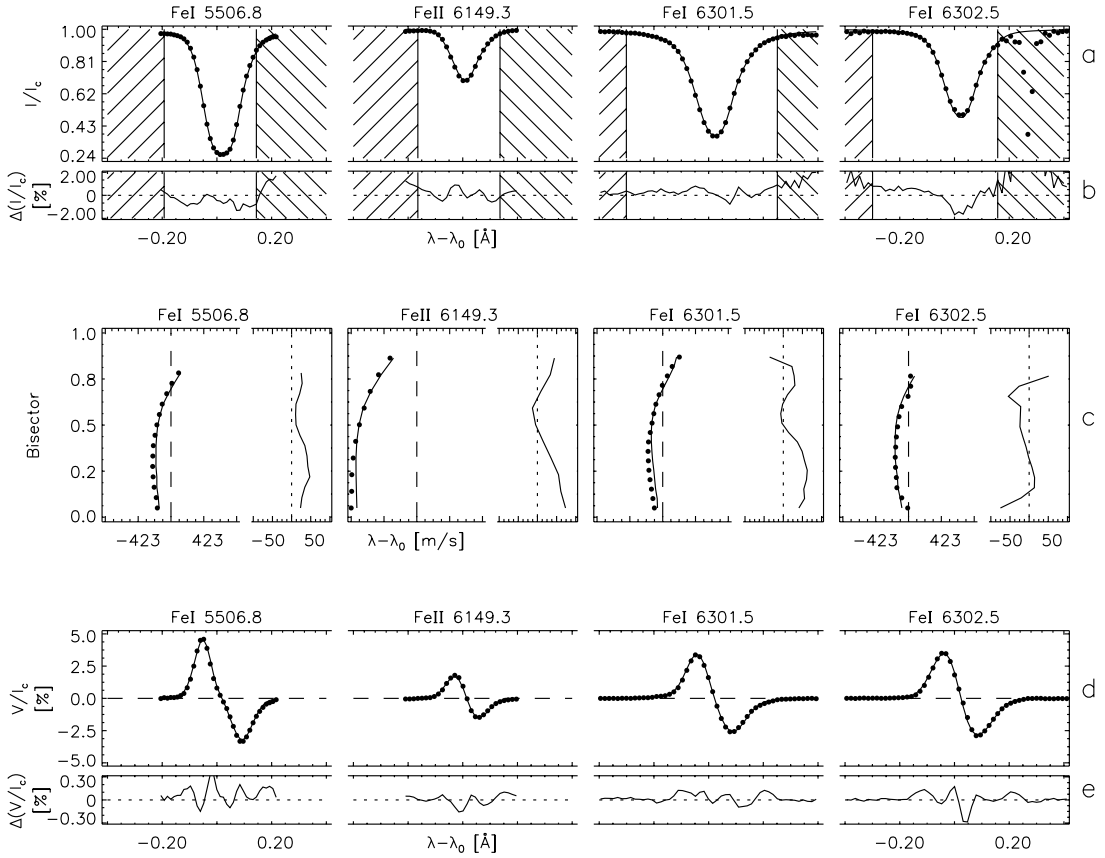

Fig. 3. Observed FTS5 profiles (dots) and overplotted best-fit profiles and bisectors (solid lines) obtained from model A. Rows **a)** and **d)** display the Stokes I and V profiles, respectively, while rows **b)** and **e)** depict the differences between the observed and synthetic profiles on a stretched scale. Row **c)** shows the line bisectors in the left part of each panel. The difference between the observed (dots) and synthetic (lines) bisectors are plotted on the right side of each panel. Dashed vertical lines indicate the reference wavelength, dashed horizontal lines in frames **b)** and **e)** the position of zero difference. The quality of the fits is equal to that to the FTS4 data, shown in Fig. 2. Therefore only four out of the 10 lines used for the inversions are shown here

FSFB99, but is extended to include both up- and downflows around the flux-tubes. In model C the velocity within the flux tube is restricted to have the same direction at all heights. In practice that means that it is directed downwards at all heights. The last column of Table 2 lists the number of free parameters in each model (not included are the free wavelength shifts for the Fe II lines, see Sect. 2). The values in brackets give the number of free parameters after a grid refinement for the depth-dependent parameters in the inversions of the FTS4 data. This was deemed reasonable due to the larger number of inverted spectral lines (including C I lines) in this data set. The total number of free parameters seems to be rather large. However, with only five free parameters to describe the depth-dependence of the temperature and velocity structure in three components one ends up with already 30 parameters free parameters. The models used for example by Bellot Rubio et al. (1997) and Almeida & Lites (2000) are based on different assumptions and use less free parameters. These models are able to reproduce the observed Stokes V asymmetries, but have not been applied to our set of spectral lines. The simultaneous inversion of up to 16 spectral lines allows us to test whether the explicitely large number of free parameters of our models can be accurately derived from the spectra.

4. Results

In the first part of this section we present the results obtained from the new 4-component model, in the second part we compare them with results obtained from the new 3-component models.

4.1. Four-component models

The observed Stokes I and V profiles for the two plage regions sampled by the FTS4 and FTS5 data sets as well as the best fits obtained with model A are shown in Figs. 2 and 3, together with the differences between the observations and fits. In Fig. 2 we show 13 of the 16 fitted lines (the quality of the fit to the remaining lines is similar). The fit to the FTS5 data is equally good, so that we restricted

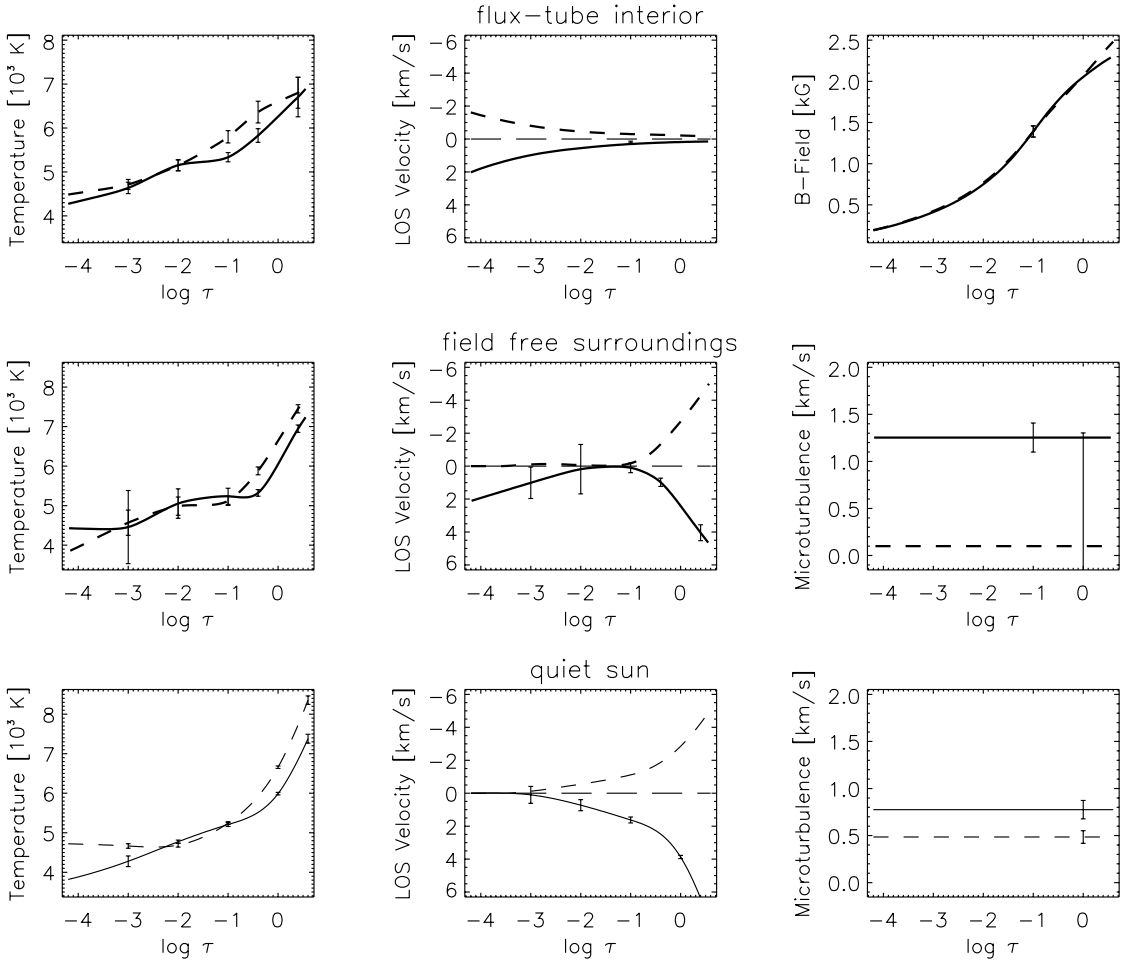

Fig. 4. Best-fit atmospheric stratifications obtained from inversions based on the 4-component model applied to FTS4 data. Solid curves correspond to components harboring downflows, dashed curves to upflowing components. From left to right we plot the deduced stratification of the temperature, line-of-sight velocity and either the magnetic field strength (top row), or the micro-turbulence (bottom two rows). The top row of panels represents the magnetic components, the middle row depicts the non-magnetic components. The bottom row shows for comparison the results obtained from inverting spectral lines of Neckel's quiet Sun atlas (see Frutiger et al. 2000). Error bars are plotted at the optical depths at which free parameters are located

Table 2. Multi-component models used for inversions

(1) Model	(2) #Comp.	(3) Characteristics	(4) M
A	4	$\boldsymbol{v}_{\rm ft2}(z) = f(z)\,\boldsymbol{v}_{\rm ft1}(z)$	41 (70)
B	3	$v_{\rm ft}(z)$	38 (67)
C	3	$v_{\rm ft}(z) \geq 0$	38 (67)

ourselves to plotting 4 of the 10 lines. For these lines we also show the observed and best-fit line bisectors (the bisectors were explicitly included in the χ^2). Note that fits to the line bisectors of the quality seen in Fig. 3 are only possible if both an up- and a downflow are allowed for in the vicinity of the flux tubes, as we ascertained. Thus the current models for the first time appear to adequately describe both the interior of the magnetic elements and their surroundings, as far as reproducing the FTS data is concerned. Only the non-hatched portion of the Stokes I profiles shown in Figs. 2 and 3 is fitted, while the whole of the plotted V profiles enters the inversions. In this way the influence of weak blends affecting the wings of the I profiles (particularly evident in Fe I 4704.9 Å and Fe I 4726.1 Å), but with no visible influence on Stokes V, can be countered. The standard error bars (representing a confidence level of 68.3%) shown in Figs. 2 and 3 are derived from the covariance matrix used in the non-linear Levenberg-Marquardt algorithm (see, e.g., Press et al. 1992). More details on the computation of reliable error estimates for a large number of best-fit parameters are given by Frutiger (2000).

Figures 4 and 5 show the corresponding best-fit stratifications of the temperature, of the magnetic field strength and of the line-of-sight velocity obtained from the new 4-component model (the quantities are plotted versus the logarithmic continuum optical depth $\tau = \tau_{5000}$ of the corresponding component).

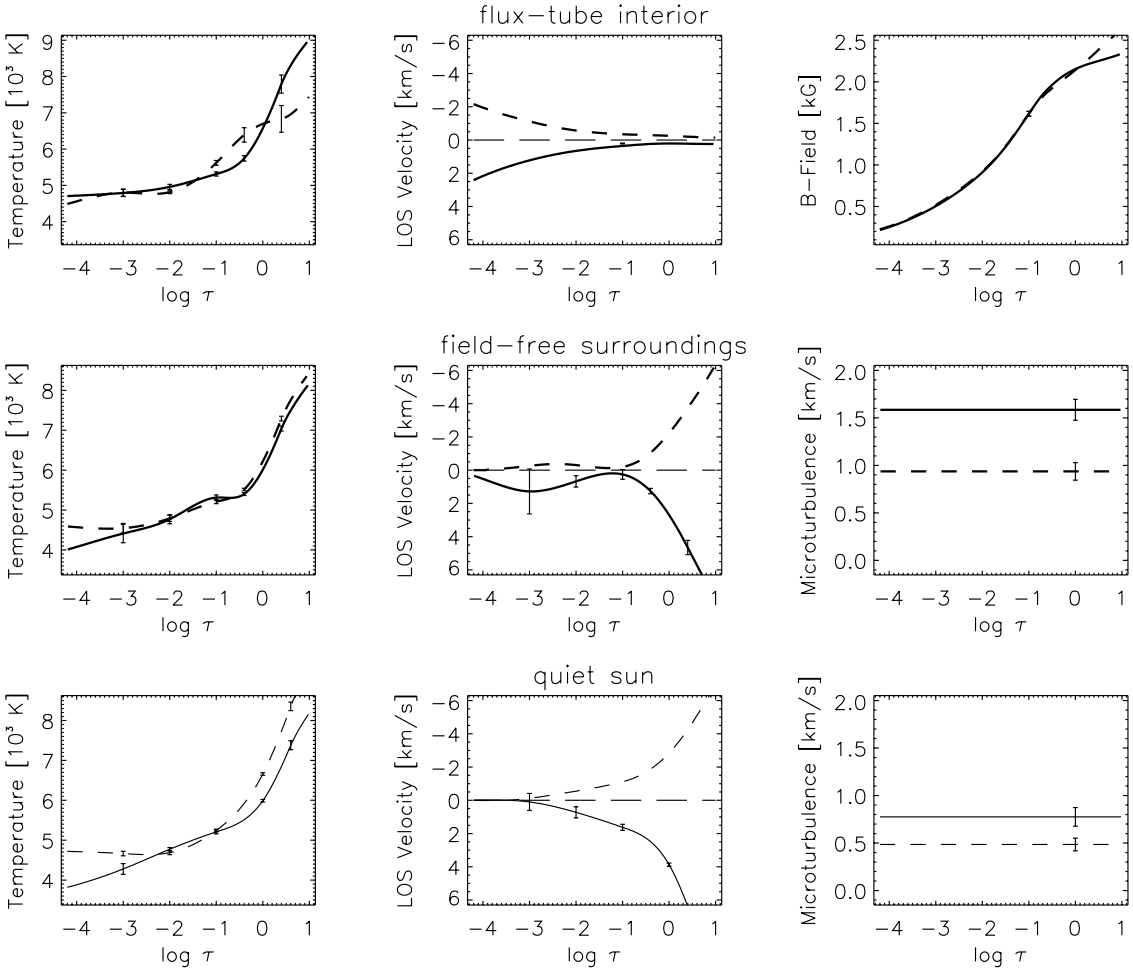

Fig. 5. Same as Fig. 4, but for the best-fit atmospheric stratification obtained from FTS5 spectra

Table 3. Best-fit (depth-independent) parameter values for multi-component models

(1) Model	(2)[1] $\alpha_{\rm ft}$	(3) $\alpha_{\rm mix}$	(4) $\alpha_{\rm hor}$	(5) $\alpha_{\rm up}$	(6) $v_{\rm mac}$ [km s^{-1}]	(7) $A_{\rm Fe}$	(8) $A_{\rm C}$	(9) χ^2
FTS4: strong plage, integration time = 35 min								
A	0.18 ± 0.02	0.55 ± 0.12	*0*	0.49 ± 0.04	1.53 ± 0.07	7.60 ± 0.03	8.54 ± 0.04	175
B	0.15 ± 0.03	–	*0*	0.37 ± 0.04	1.65 ± 0.08	7.64 ± 0.02	8.53 ± 0.04	196
C	0.15 ± 0.02	–	*0*	0.37 ± 0.04	1.68 ± 0.08	7.64 ± 0.02	8.53 ± 0.04	219
FTS5: strong plage, integration time = 21 min								
A	0.15 ± 0.05	0.53 ± 0.01	*0*	0.53 ± 0.03	1.16 ± 0.06	7.39 ± 0.03	–	74
B	0.16 ± 0.02	–	*0*	0.53 ± 0.03	1.46 ± 0.05	7.45 ± 0.02	–	86
C	0.16 ± 0.02	–	*0*	0.53 ± 0.04	1.51 ± 0.05	7.45 ± 0.02	–	154

[1] At reference height $z = 0$ which corresponds to the reference depth $\log \tau_{5000} = 0$ in the vicinity of the magnetic flux tubes.

The remaining depth-independent best-fit parameters together with the χ^2 of the best fits are listed in Table 3. Column (2) gives the fraction of the area covered by a magnetic field (at the reference height $z = 0$ within the flux tube which corresponds to depth $\tau_{5000} = 1$ in the non-magnetic surroundings) for a 2-component thin-tube model composed of the magnetic flux-tube interior and the non-magnetic surroundings harboring a downflow. The magnetic filling factor of the full model is given by $\alpha_{\rm ft}\,(1-\alpha_{\rm up})$ (see Eq. (1)) and thus turned out to be about 0.1 for the FTS4 data and 0.07 for the FTS5 data. Column (3) displays the weight associated with the second type of flux tubes (see Eq. (2)). Column (4) lists the surface fraction harboring a horizontal flow (prescribed to be zero) while the contribution of the non-magnetic area harboring an upflow is given in Col. (5). Column (6) lists

the macro-turbulence, Cols. (7) and (8) the iron and carbon abundances (on the usual scale where the hydrogen abundance $A_{\rm H} = 12$). Finally, the last column gives the best-fit normalized χ^2 returned by the inversion code (see Frutiger et al. 2000 for details).

In both plage regions the area covered by the upflow is slightly larger than the downflow area ($\alpha_{\rm down} = (1-\alpha_{\rm up})(1-\alpha_{\rm ft})$), as can be deduced from Table 3. Inversions carried out with $\alpha_{\rm hor}$ a free parameter revealed no need for a significant surface fraction harboring a horizontal flow, so that we set $\alpha_{\rm hor}$ to zero in the models presented here. The comparison with the best-fit stratifications obtained from inversions of quiet-sun spectra (Frutiger et al. 2000, see bottom row in Figs. 4 and 5) suggests that in the granulation of the plage area the temperature contrast between the up- and downflow (i.e. also the continuum contrast) is lower, the vertical velocities in the lower photosphere are smaller and the asymmetry between upward and downward flow speeds in the granulation is less pronounced (which also implies that the fractions of the surface harboring an up- and downflow are more similar) relative to the quiet sun. Also, the turbulent velocities are larger in the active region granules (cf. Nesis et al. 1993). This correspondence between the properties of the convective cells returned by the inversion and those of abnormal granulation is close (e.g. Title et al. 1992), see however Sect. 5.

The stratification of physical parameters inside the magnetic elements are given in the top row of panels of Figs. 4 and 5. At first sight the results obtained for the two plage regions are qualitatively similar. There are differences between the stratification of the temperature, however, in particular for the continuum forming layers, as discussed in Sect. 5. From the tests described there we conclude that the stratification derived from the FTS4 data is more reliable. From both the FTS4 and FTS5 data we obtain that about one half of the flux tubes harbor an upflow (or all flux tubes harbor an upflow half of the time) while the other half harbors a similar downflow.

The vertical stratification of the velocity is determined by mass conservation with height. This form was chosen in order to restrict the number of free parameters and may well not be the ideal form to reproduce the observations. The height dependence obviously depends on the number of spectra and lines fitted (compare FS98 with FSFB99) and the type of model and constraints imposed (compare FSFB99 and the current paper). Obviously the synthetic spectra react mainly to the fact that two magnetic components with oppositely directed velocities are present (see Solanki (1989) and Grossmann-Doerth et al. (1991) and far less to the exact stratification of these velocities.

BRC99 proposed to use the Stokes V zero crossing wavelength shifts of more than 100 Fe I lines in the same spectrum from which the lines for the inversions have been taken in order to test the predictive power of the fits. We have applied this test to our inversions as well. The comparison between the observed values and those obtained from the synthesis using the best-fit model atmosphere are presented in Fig. 8. With only a few exceptions the 4-component model is able to reproduce the observed Stokes V zero-crossing shifts within the estimated errors in the laboratory reference wavelengths. Note also that the scatter visible in Fig. 8 is on the same order as that obtained when plotting the observed wavelengths shifts against another observable, e.g. line strength (Solanki 1986, Fig. 1a).

The iron abundance is treated as a free parameter in order to investigate whether the inversions are able to accurately determine this quantity from our different lists of spectral lines. The results returned by the inversions show that the simultaneous determination of the temperature structure (in several components) and the Fe abundance has its limitations. Additional calculations with $A_{\rm Fe}$ fixed to 7.5 (not presented here) revealed that the high values of $A_{\rm Fe}$ for FTS4 are compensated for by slightly cooler temperature stratifications (within the range of the given error bars), whereas the low $A_{\rm Fe}$ in FTS5 leads to slightly hotter temperatures as those returned for $A_{\rm Fe} = 7.5$. In all cases the fits to the observations with the Fe abundances treated as a free parameter were about 10–20% better than the fits with fixed iron abundance.

4.2. Three-component models

In this section we discuss inversions restricted to three components, i.e. to a single flux tube. Such 3-component inversions allow us to test whether we can distinguish between the two types of models on the basis of the fits or of physical considerations. New inversions of this type are needed in order to take into account the influence of the improved treatment of the field-free atmosphere on the fit to the observed data and on the deduced atmospheric stratifications, in particular the velocities inside the magnetic flux tube.

First we present the results obtained from the inversions with free velocities inside the magnetic flux tube (model B in Table 2, corresponding closest to the model of BRC97). The best-fit atmospheres obtained from inverting the FTS4 and FTS5 spectra are shown in Figs. 6 and 7, respectively. The remaining depth-independent parameters are listed in Table 3. As far as the magnetic component is concerned the results, in particular those for FTS5 agree well with the findings of BRC97 (recall that the lines they inverted, Fe I 6301.5 Å and 6302.5 Å, fall within the wavelength range of FTS5). The observed Stokes V zero-crossing wavelengths of more than 100 Fe I lines from FTS5 and those derived from the synthetic profiles calculated using the best-fit atmospheres are presented in Fig. 9 (filled circle). They further confirm the results presented by BRC99. The best-fit profiles are not shown again, since the quality of the fits is close to that seen in Figs. 2 and 3. The χ^2 of the fits is again excellent (Table 3).

It is disturbing, however, that the velocity within the flux tube changes sign in the lower photosphere in both these inversions. Hence there is a strong downflow below this level and a weaker upflow above it. Within the context

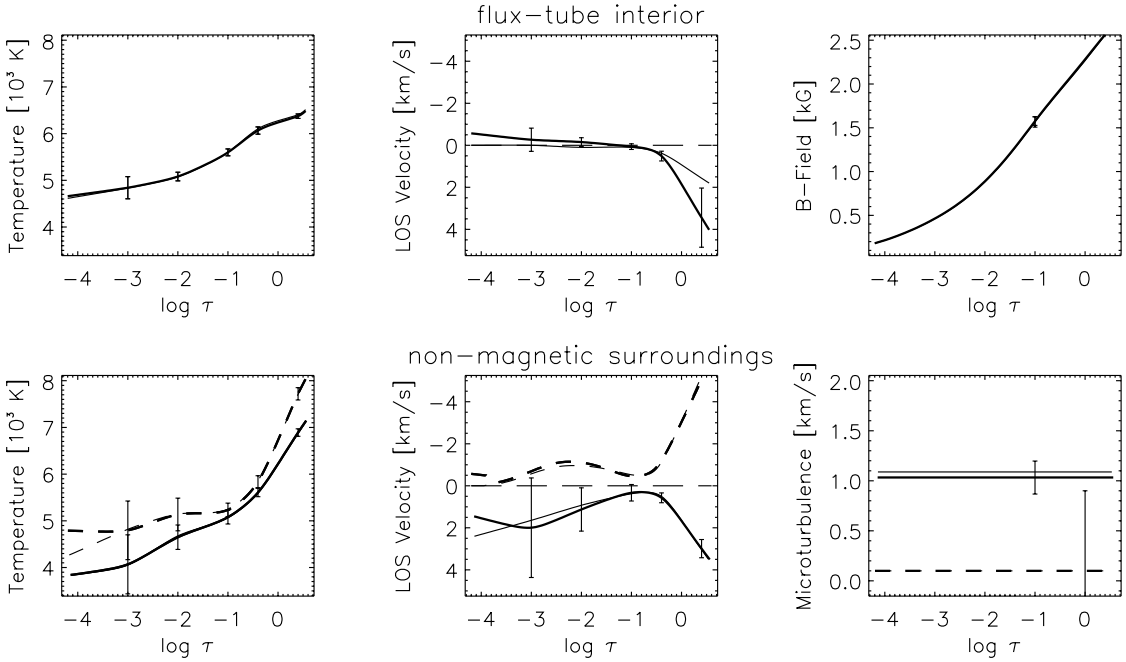

Fig. 6. Same as Fig. 4, but for best-fit atmospheric stratifications obtained from 3-component models B (thick curves) and C (thin curves, practically identical to model B, except for the velocity inside the magnetic flux tube). In model C only downflows (positive velocities) are allowed inside the magnetic elements

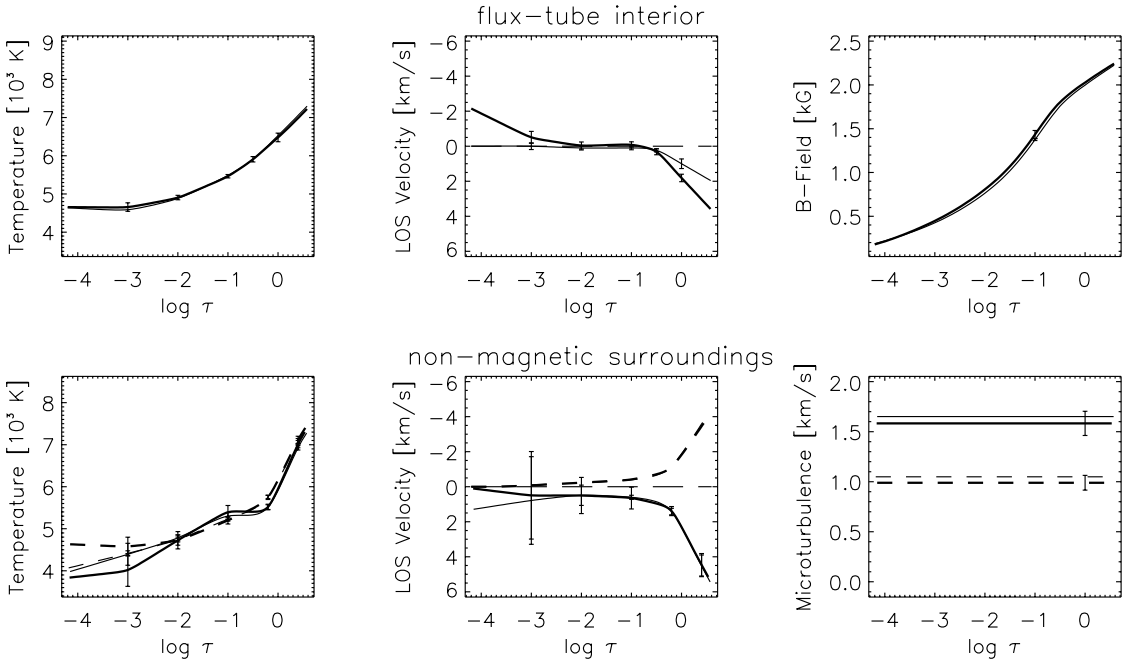

Fig. 7. Same as Fig. 6, but for best-fit atmospheric stratifications obtained from FTS5 plage spectra (including the two ASP lines Fe I 6301.5 Å and Fe I 6302.5 Å)

of a topologically simple magnetic configuration, as used here, this velocity structure does not make physical sense, in particular since the gas flow across field lines is insufficient by orders of magnitude to feed such diverging vertical flows (Hasan & Schüssler 1985). Therefore, we redid the inversion using model C, which is identical to model B, except that the velocity is forced to have the same sign at all heights (only a downflow turns out to be reasonable). The stratifications resulting from this model are plotted in Figs. 6 and 7 (thin curves). With the exception of the internal velocity, they are almost identical to those found with model B, which is encouraging. However, not

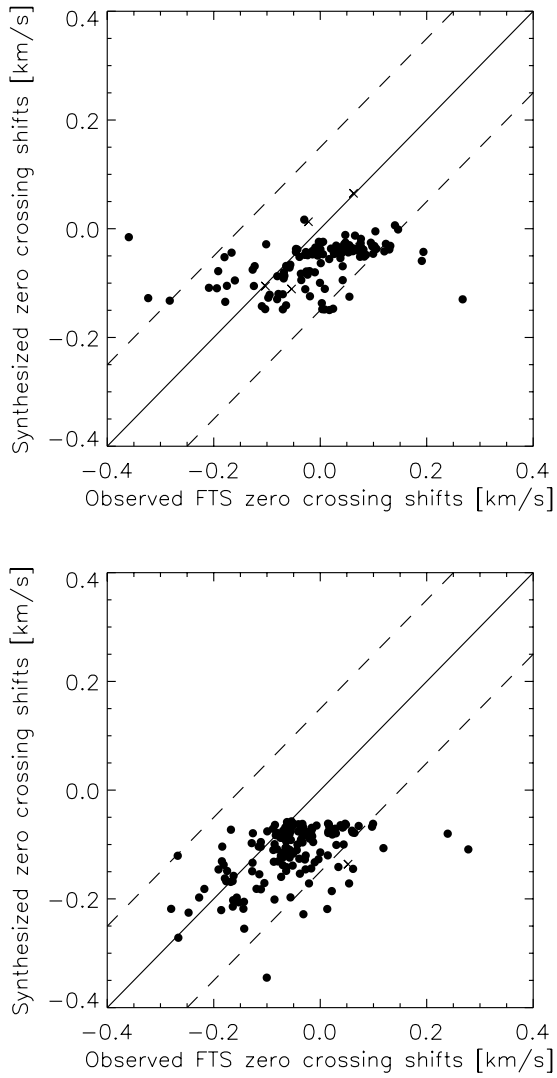

Fig. 8. Synthetic versus observed Stokes V zero crossing wavelengths shifts (in velocity units) of more than 100 Fe I lines in the data set FTS4 (upper panel) and FTS5 (lower panel). The synthetic profiles are calculated from the best-fit 4-component model A. The slanted lines indicate where to points would lie if the observed on synthetic shifts were equal (solid) and the uncertainty introduced by the estimated standard errors in the laboratory wavelengths (dashed). The crosses refer to the spectral lines used in the inversions.

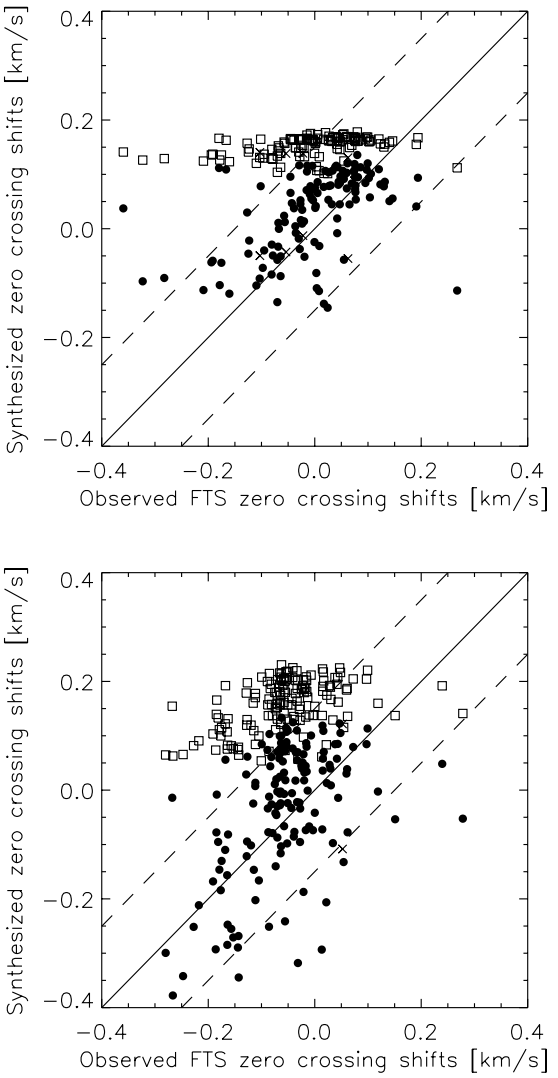

Fig. 9. Same as Fig. 8, but for synthetic Stokes V zero-crossing wavelength shifts obtained from the best-fit 3-component models B (dots) and C (open squares). The upper panel refers to spectral lines in the FTS4 dataset, the lower panel to FTS5

allowing flows directed in opposite directions in the flux-tube interior leads to a considerably poorer fit, in particular for FTS5 (larger χ^2; see Table 3). Also the Stokes V zero-crossing wavelength shifts show large deviations from the observed ones, in excess of the uncertainty for many lines (Fig. 9, open squares). This model is therefore inferior to the others.

5. Continuum brightness and contrast

The inversions presented here are based on normalized data. I.e. they are not constrained to reproduce the correct continuum intensity, I_c. Here we discuss the I_c predicted by the best-fit models.

When inverting the FTS4 data we have in general included three weak high-excitation C I lines (see Table 1) that are sensitive to the temperature close to the $\tau_{5000} = 1$ level (Livingston et al. 1977; Elste 1985) with the goal of better constraining the temperature of the continuum-forming layers in the magnetic elements (Solanki & Brigljević 1992) and their surroundings.

The continuum intensities (calculated at the wavelength of the first spectral line for a particular data set, see Table 1) and contrasts obtained from these inversions are listed in the top rows of Table 4. The name of the model is tabulated in Col. (1). $A_{\rm up}$ and $A_{\rm dn}$ refer to the different types of flux tubes (up- and downflow in the tube interior, but common surroundings). Column (2) lists the continuum contrast of the flux-tube core to the spatially averaged continuum intensity, $\delta_{\rm m} = I_{\rm m}/I_0$. The flux-tube core is composed of that part which can be represented by a single-component magnetic atmosphere down to $\tau = 10$,

Table 4. Continuum intensities and contrasts

(1) Model	(2) $\delta_{\rm m}$	(3) $\delta_{\rm ft}$	(4) $\delta_{\rm dn}$	(5) $\delta I_{\rm rms}$	(6) $\delta I_{\rm rms,nm}$	(7) $\delta_{\rm gs}$
FTS4 + C I lines						
$A_{\rm dn}$	0.88	1.03	0.80	0.18	0.15	0.92
$A_{\rm up}$	1.11	1.15	0.80	0.17	0.15	0.94
$A_{\rm avg}$	0.99	1.09	0.80	0.18	0.15	0.93
B	0.85	1.06	0.83	0.20	0.17	0.95
C	0.87	1.07	0.83	0.20	0.17	0.95
FTS4, no C I lines						
$A_{\rm dn}$	1.18	1.35	0.93	0.15	0.05	0.86
$A_{\rm up}$	1.37	1.41	0.93	0.15	0.05	0.86
$A_{\rm avg}$	1.28	1.38	0.93	0.15	0.05	0.86
B	1.30	1.41	0.94	0.15	0.04	0.92
C	1.26	1.40	0.94	0.15	0.04	0.91
FTS5, no C I lines						
$A_{\rm dn}$	1.25	1.32	0.91	0.14	0.06	0.86
$A_{\rm up}$	1.23	1.29	0.91	0.13	0.06	0.86
$A_{\rm avg}$	1.24	1.31	0.91	0.14	0.06	0.86
B	1.15	1.24	0.93	0.12	0.04	0.84
C	1.21	1.23	0.91	0.11	0.05	0.82
3-comp quiet sun (Frutiger et al. 2000)						
F	–	–	–	–	0.18	0.97

i.e. the part of the flux tube with the maximum Wilson depression. Column (3) shows the continuum contrast of the central cylinder of the flux tube to the average plage, $\delta_{\rm ft} = I_{\rm ft}/I_0$. The central cylinder is defined as the parts of the flux tube for which $\tau = 1$ lies within the flux tube or at its edge, i.e. it is composed of the flux-tube core and the neighboring hot walls. Column (4) shows the continuum contrast of the moat around the flux tube to the average plage, $\delta_{\rm dn} = I_{\rm dn}/I_0$. For our models, the moat is defined as the non-magnetic surroundings harboring a downflow without the hot walls that contribute to $\delta_{\rm ft}$. Column (5) lists the rms contrast of the intensity pattern defined as $\delta I_{\rm rms} = \sqrt{\sum_i f_i \, (\frac{I_i}{I_0} - 1)^2}$, where f_i is the fractional area having intensity I_i and $I_0 = \sum_i f_i \, I_i$ is the average intensity of the observed plage area (the summation is carried out over the 22 rays of our modified thin-tube models). Column (6) shows the rms contrast if the flux-tube central cylinder is not included in the weighted sum over the intensity variations. This quantity thus is a measure of the granular rms contrast in the plage. Finally Col. (7) contains the ratio, $\delta_{\rm gs} = I_0/I_{\rm gs}$, of the average continuum intensity of the best-fit model to the continuum intensity obtained from the calculation of spectra for the 1-dimensional standard solar atmosphere of Grevesse & Sauval (1999).

The temperature contrast between the up- and downflow (i.e. also the continuum contrast) is lower in the granulation of the plage region than in the quiet sun (see Col. 6 of Table 4; model F refers to the 3-component quiet-sun model F of Frutiger et al. 2000). This result agrees well with the findings of Title et al. (1992). The inclusion of the C I lines leads to a considerable decrease in the flux-tube brightness in good agreement with the findings of Solanki & Brigljević (1992). When the effect of the hot walls is included the flux tubes are found to be slightly brighter than the average quiet Sun and surrounded by a dark moat which compensates the brightness enhancement in the continuum due to the hot walls. This also appears to agree reasonably well with the results of Topka et al. (1992), but a comparison with their observations is not so straightforward due to the extreme sensitivity of the rms contrast to seeing (Title & Berger 1996).

Column 7 reveals that the spatially integrated continuum intensity of the plage models is about 6% smaller than the continuum intensity of the average quiet-sun models of Maltby et al. (1986) or Grevesse & Sauval (1999). Contrast measurements of plage at low spatial resolution, however, return contrast values close to zero (e.g. Foukal & Fowler 1984). An uncertainty of 6% in the continuum intensity corresponds to an uncertainty of about 150 K in the temperature of the continuum forming layers. The error estimates obtained from the inversions for the temperature in these layers are just of this order of magnitude (see error bars in Figs. 4 and 5). This indicates the limits of accuracy achievable with fits to normalized line profiles, and suggests the need to fit the absolute intensity spectra in future or include the (spatially averaged) continuum contrast separately in the inversion.

In order to estimate how important the C I lines are to constrain the temperature in the continuum forming layers within the flux tubes we also inverted the FTS4 data, but without the C I lines. The contrasts are given in the middle part of Table 4. The flux tubes are now considerably brighter and the granular contrast is very much lower. Also, $\delta_{\rm gs}$ the spatially averaged contrast is lower.

The inversions of the FTS5 data set, which contains no C I lines, confirm the above behavior. These data also return a strong flux-tube contrast and a low $\delta_{\rm gs}$. This not only suggests that the C I lines provide important constraints on the flux-tube temperature, but also that the temperature stratification obtained from FTS4 (Fig. 4) is to be trusted more than that deduced from FTS5 (Fig. 5). Other parameters, in particular the velocity structure are only slightly sensitive to the continuum level. Thus any remaining uncertainties in the continuum level are not expected to influence the main conclusions of this paper.

6. Discussion and conclusions

We have demonstrated that our new 3- and 4-component flux-tube models can satisfactorily reproduce the observed Stokes I and V profiles of neutral and singly ionized iron spectral lines in plage regions. The 3-component model has a steady flow inside the flux-tube component while in the 4-component case the flows are oppositely directed in the 2 flux-tube components (which could represent opposite phase of an oscillation). For the first time the Stokes I

line bisectors in an active region are also well fit by the inversion. In addition, the best-fit atmospheres returned by the inversions are able to reproduce the observed Stokes V zero-crossing wavelength shifts of more than 100 unblended Fe I lines in the two FTS spectra from which 16 respectively 10 lines have been used in the inversions. Thus the result found by FS98 that the observations provide no clear-cut preference for one of these models still holds for the more realistic models used here. An exception is the 3-component model if we require it to have only downflows inside the magnetic element. In this case the fit is of considerably poorer quality.

One gratifying aspect of the new models, when applied to spectra of Fe I, Fe II and C I lines, is that the properties of the granular convection in active region plage which they return are similar to those expected for abnormal granulation. In particular, we find that the granular up- and downflow velocity is reduced while the turbulent velocity is increased in the plage intergranular lanes. This agrees well with the findings obtained from high-resolution spectra that in active regions the granular velocity shifts almost disappear, but that the lines are somewhat broadened (e.g. Nesis et al. 1993). Also, we find that the continuum brightness and contrast are in reasonable agreement with the observations only if lines formed deep in the atmosphere, such as the C I lines, are included. The spatially averaged continuum intensities are nevertheless slightly too small. If spectral lines that are particularly sensitive to the temperature of the continuum forming layers are not available, as in the case of the FTS5 data, the results of the χ^2 based inversion technique applied to normalized spectral line profiles decline in reliability.

The 4-component model is constrained to achieve mass conservation as a function of height within the flux tubes (i.e. the same amount of mass flows through the flux-tube's cross-section at different heights), but also at a given height when averaged over different flux tubes within the resolution element or time (what flows up through a flux-tube cross-section at a given height must flow down again in another flux tube or at a later time). Note that the former constraint is not strictly needed from a physical point of view, and is only imposed to reduce the number of free parameters. The characteristic Stokes V asymmetries observed in plage regions are already present in spectra whose integration time is just a few seconds (see, e.g., Grossmann-Doerth et al. 1996; Pillet et al. 1997). This time interval is simply too short for a significant dynamical evolution of the flux tubes. Thus, if mass conservation holds for these short intervals, then the two types of flux tubes in the 4-component model are rather to be interpreted as coexisting unresolved flux tubes (harboring an up- and downflow) than associated with two phases of an oscillatory motion, unless we are dealing with body modes having radial nodes in the interior of the flux tube. For the FTS spectra considered here, however, the long integration time may in addition also average over oppositely directed flows inside magnetic elements at different times.

The main problem faced by the 3-component models is mass conservation. The comparison between the two presented models of this type reveals clear differences once physical constraints are imposed. For example, the best fit (to the observed Stokes I and V profiles and in particular to the observed Stokes V zero-crossing wavelengths shifts) is achieved only if the velocity changes sign at a given height in the photosphere. Taking into account that mass cannot flow across field lines to the extent needed here (Hasan & Schüssler 1985) and also the long time (21–35 min) and spatial area sampled by the observations we conclude that the 3-component model is not appropriate for this type of data. A concurrent upflow in the upper layers of the flux tubes and downflow in the deeper layers would evacuate the flux-tube in a fraction of the observed time. It is, of course conceivable that magnetic field topologies are present over at least a part of a flux tube's life time which allow a flow field of the type found by model B to be present (e.g. sideways connection of flux tubes, etc.). Indeed, the simulations of Ploner et al. (2001) do reveal such situations in the course of the evolution of some magnetic elements. However, this is not the norm. Nevertheless, a comparison with such simulations reminds us that the true structure of flux-tubes could be far more complex than we model.

A different approach is the MISMA scenario by Almeida & Lites (2000) based on magnetic structures far smaller than the horizontal photon mean free path in the photosphere. Our work shows that flux-tubes of "classical" size (i.e. diameters of 100 km or more) reproduce the observations very well. Mass conservation is not treated as strictly in the investigations of MISMAS to date as in our models.

For small resolution elements and short integration times imposing mass conservation, however, does not necessarily represent a real improvement. It may turn out to be inadequate if the flow connects different resolution elements. On the other when looking at small scale structures it is important not to forget the global physical constraints. If flux tubes are proposed to harbor downflows, then this massflow must be balanced with corresponding upflows at some point in space or time. The MISMA model as well as our multi-component models have to demonstrate more stringently whether they can reproduce a wide variety of data, e.g. spectra with different spatial and temporal resolution, while taking into account the large scale mass conservation constraints. In our future work we plan to extend this analysis to observations made near the solar limb which may reveal new insights into the structure and dynamic behavior of small-scale magnetic elements.

Acknowledgements. This research was supported by the Swiss Nationalfonds under NF grant No. 20-50464.97.

References

Anstee, S. D., & O'Mara, B. J. 1995, MNRAS, 276, 859
Bard, A., Kock, A., & Kock, M. 1991, A&A, 248, 315

Bard, A., & Kock, M. 1994, A&A, 282, 1014
Barklem, P. S., & O'Mara, B. J. 1997, MNRAS, 290, 102
Barklem, P. S., O'Mara, B. J., & Ross, J. E. 1998, MNRAS, 296, 1057
Bellot Rubio, L. R., Ruiz Cobo, B., & Collados, M. 1997, ApJ, 478, L45
Bellot Rubio, L. R., Ruiz Cobo, B., & Collados, M. 1998, ApJ, 506, 805
Bellot Rubio, L. R., Ruiz Cobo, B., & Collados, M. 1999, A&A, 341, L31
Bernasconi, P. N., Keller, C. U., Povel, H. P., & Stenflo, J. O. 1995, A&A, 302, 533
Briand, C., & Solanki, S. K. 1998, A&A, 330, 1160
Bünte, M., Solanki, S. K., & Steiner, O. 1993, A&A, 268, 736
Defouw, R. J. 1976, ApJ, 209, 266
Elste, G. 1985, in Theoretical Problems in High Resolution Solar Physics, ed. H. Schmidt, Max-Planck-Inst. f. Astrophysik, 185
Foukal, P., & Fowler, L. 1984, ApJ, 281, 442
Frutiger, C. 2000, Ph.D. Thesis, ETH Zürich, No. 13896
Frutiger, C., & Solanki, S. K. 1998, A&A, 336, L65
Frutiger, C., Solanki, S. K., Fligge, M., & Bruls, J. H. M. J. 1999, in Solar polarization, ed. K. N. Nagendra & J. O. Stenflo (Dordrecht: Kluwer), 281
Frutiger, C., Solanki, S. K., Fligge, M., & Bruls, J. H. M. J. 2000, A&A, 358, 1109
Fuhr, J. R., Martin, G. A., & Wiese, W. L. 1988, J. Phys. Chem. Ref. Data, 17, Suppl. 4
Grevesse, N., & Sauval, A. J. 1999, A&A, 347, 348
Grossmann-Doerth, U., Keller, C. U., & Schüssler, M. 1996, A&A, 315, 610
Grossmann-Doerth, U., Schüssler, M., & Solanki, S. K. 1989, A&A, 221, 338
Grossmann-Doerth, U., Schüssler, M., & Solanki, S. K. 1991, A&A, 249, 239
Grossmann-Doerth, U., Schüssler, M., & Steiner, O. 1998, A&A, 337, 928
Gustafsson, B. 1973, Uppsala Astron. Obs. Ann., 5
Hasan, S., & Schüssler, M. 1985, A&A, 151, 69
Illing, R. M. E., Landman, D. A., & Mickey, D. L. 1975, A&A, 41, 183
Kurucz, R. L., & Bell, B. 1995, Harvard-Smithsonian Center for Astrophysics, CD-ROM, No. 23
Landi Degl'Innocenti, E. 1976, A&A, 25, 379
Livingston, W., Milkey, R., & Slaughter, C. 1977, ApJ, 211, 281
Maltby, P., Avrett, E. H., Carlsson, M., et al. 1986, ApJ, 306, 284
Márquez, I., Bonet, J. A., & Vázquez, M. 1996, A&A, 306, 305
Martínez Pillet, V., Lites, B. W., & Skumanich, A. 1997, ApJ, 474, 810
Mathys, G. 1990, A&A, 236, 527
Miller, M. H., Wilkerson, T. D., Roig, R. A., & Bengston, R. D. 1974, J. Phys. Chem. Ref. Data A, 9, 2312
Moore, C. E. 1970, NSRDS-NBS, Sect. 3
Nave, G., Johansson, S., Learner, R. C. M., Thorne, A. P., & Brault, J. W. 1994, ApJS, 94, 221
Nesis, A., Hanslmeier, A., Hammer, R., et al. 1993, A&A, 279, 599
Ploner, S. R. O., Schüssler, M., Solanki, S. K., & Gadun, A. S. 2001, in Advanced Solar Polarimetry: Theory, Observation, and Instrumentation, ASP Conf. Ser., ed. M. Sigwarth, submitted
Press, W. H., Teukolsky, S. A., Vetterling, W. T., & Flannery, B. P. 1992, Numerical Recipies in Fortran, 2nd edn. (New York: Cambride University Press)
Rees, D. E., Murphy, G. A., & Durrant, C. J. 1989, ApJ, 339, 1093
Ruiz Cobo, B., & Del Toro Iniesta, J. C. 1992, ApJ, 398, 375
Sánchez Almeida, J. 1997, ApJ, 491, 993
Sánchez Almeida, J., Collados, M., & Del Toro Iniesta, J. C. 1989, A&A, 222, 311
Sánchez Almeida, J., & Lites, B. W. 2000, ApJ, 532, 1215
Schnabel, R., Kock, M., & Holweger, H. 1999, A&A, 342, 610
Sigwarth, M., Balasubramaniam, K. S., Knölker, M., & Schmidt, W. 1999, A&A, 349, 941
Solanki, S. K. 1986, A&A, 168, 311
Solanki, S. K. 1987, Ph.D. Thesis, ETH Zürich, No. 8309
Solanki, S. K. 1989, A&A, 224, 225
Solanki, S. K., & Brigljević, V. 1992, A&A, 262, L29
Solanki, S. K., & Stenflo, J. O. 1985, A&A, 148, 123
Steiner, O., Grossmann-Doerth, U., Knölker, M., & Schüssler, M. 1998, ApJ, 495, 468
Stenflo, J. O., Solanki, S. K., Harvey, J. W., & Brault, J. W. 1984, A&A, 131, 333
Sugar, J., & Corliss, C. 1985, J. Phys. Chem. Ref. Data, 14, Suppl 2
Title, A. M., & Berger, T. E. 1996, ApJ, 463, 797
Title, A. M., Topka, K. P., Tarbell, T. D., et al. 1992, ApJ, 393, 782
Topka, K. P., Tarbell, T. D., & Title, A. M. 1992, ApJ, 396, 351